11th AIAA/CEAS Aeroacoustics Conference (26th AIAA Aeroacoustics Conference)
23 - 25 May 2005, Monterey, California

AIAA 2005-2996

The Calculation of Acoustic Shielding of Engine Noise by the Silent Aircraft Airframe

Anurag Agarwal* and Ann P. Dowling†

University of Cambridge, Trumpington Street, Cambridge CB2 1PZ, UK

The Silent Aircraft airframe has a flying wing design with a large wing planform and a propulsion system embedded in the rear of the airframe with intake on the upper surface of the wing. In the present paper, boundary element calculations are presented to evaluate acoustic shielding at low frequencies. Besides the three-dimensional geometry of the Silent Aircraft airframe, a few two-dimensional problems are considered that provide some physical insight into the shielding calculations. Mean flow refraction effects due to forward flight motion are accounted for by a simple time transformation that decouples the mean-flow and acoustic-field calculations. It is shown that significant amount of shielding can be obtained in the shadow region where there is no direct line of sight between the source and observer. The boundary element solutions are restricted to low frequencies. We have used a simple physically-based model to extend the solution to higher frequencies. Based on this model, using a monopole acoustic source, we predict at least an 18 dBA reduction in the overall sound pressure level of forward-propagating fan noise because of shielding.

I. Introduction

The "Silent Aircraft Initiative" is a project funded by the Cambridge-MIT Institute (CMI). Its aim is to discover ways of reducing aircraft noise to the point where it would be virtually imperceptible to people outside the airport perimeter in a typical urban environment. The present design of the Silent Aircraft is in the form of a flying wing with a large wing planform and a propulsion system that is embedded in the rear of the airframe with intake on the upper surface of the wing. Thus a large part of the forward-propagating noise from the intake duct of the engines is shielded by the wing from observers on the ground.

Acoustic shielding estimates of noise from engines placed above a wing have been obtained by a few investigators in the past, experimentally and numerically, for both tube-and-wing and flying-wing aircraft configurations. For example, Jeffery and Holbeche[1] studied the acoustic shielding from a full scale Hadley-Page 115 delta-winged aircraft in flight by centrally mounting a powerful acoustic whistle above the wing. They also performed experiments on a model scale aircraft mounted in a wind tunnel. They observed significant amount of shielding in the shadow region. They developed a simple model based on diffraction from a sharp-edged semi-infinite plate to predict the noise underneath the wing. Clark and Gerhold[2] experimentally investigated the noise shielding by a 3-engine Blended-Wing-Body (BWB) model. A high-frequency broadband point source was placed in the nacelles of the engines. They observed shielding in excess of 20 dB for the Overall Sound Pressure Level (OASPL) in the forward sector of the shadow region. The amount of shielding in the aft sector was relatively smaller, of the order of 10 dB. This is because both exhaust and inlet radiated noise contributed to their result. Gerhold et al.[3] used a simple wedge-shaped wing with a triangular planform and a point source mounted in a nacelle above the wing, in order to compare experimental results

---

*Research Associate, Department of Engineering, AIAA Member
†Professor, Department of Engineering, AIAA Member

with a numerical model. They used a boundary integral method to perform low-frequency calculations and found good qualitative agreement with the experimental results. Ricouard et al.[4] studied the shielding of fan noise by the main wing of a scaled model tube-and-wing aircraft. In their experiments, the engine was mounted over the tail wing. In this situation shielding is effective only in certain directions underneath the wing along which there is no direct line of sight between the engine-intake and observers on the ground. All these experimental investigations show a significant amount of shielding in the shadow zone underneath the aircraft. Numerical solutions for realistic aircraft models so far have yielded only qualitative results and provide little physical insight into the acoustic shielding solutions. Most theoretical models developed so far use diffraction theories based on acoustic scattering from a semi-infinite plate, which, as is shown in a subsequent section, is applicable only under certain conditions. Also most models and numerical simulations have ignored mean flow refraction effects.

In the present paper, low-frequency acoustic shielding estimates are obtained from a point monopole source placed above simple two-dimensional geometries and a three-dimensional Silent Aircraft model. The analysis accounts for mean flow refraction effects due to forward flight motion and provides a framework for incorporating realistic acoustic sources. The two-dimensional models provide some physical insight into acoustic shielding calculations. For example, these models help explain the effect of various parameters such as wing thickness, edge curvatures, source frequency, etc. on the amount of acoustic shielding. These models also help in identifying the relevant length and frequency scales of the problem, which is useful in developing simple analytical models.

Acoustic shielding effects can be calculated by solving an external acoustic scattering problem. Acoustic waves generated by the engines are refracted by the mean flow past the moving aircraft. Considerable simplifications to this problem can be made for low-Mach number flows (where $|\boldsymbol{M}|^2$ is negligible, $\boldsymbol{M}$ being the Mach number) that can be assumed to be homentropic and potential. This assumption is valid for flows with high Reynolds numbers in which boundary layer separation does not occur, such as the flow-field around an airfoil (slender body moving parallel to its length) at low angles of attack. Taylor[5] introduced a coordinate transformation by which the governing acoustic equations in a steady low-Mach number homentropic potential flow are transformed into an ordinary wave equation. Taylor[5] developed this transformation to aid aircraft noise measurements from wind-tunnel and low-speed flight tests. Taylor's transformation distorts the time variable and thereby decouples the mean-flow and acoustic equations. This is shown in section II for external source scattering problems. Thus the effect of a background flow-field on sound propagation can be obtained by solving, independently, the potential (Laplace) equation for steady fluid flow, and the Helmholtz equation for acoustic-wave propagation in the transformed time variable, and then transforming the result into the physical time variable. Astley and Bain[6] used Taylor's transform in a similar way to arrive at the governing acoustic equations suitable for the solution of Neumann boundary-value problems by boundary element methods. Numerical solvers based on boundary element methods are readily available for both Helmholtz and Laplace equations. Thus existing boundary element solvers can be used to solve the problem of sound propagation through low-Mach number homentropic potential flows. A boundary element implementation by means of an example of acoustic scattering from a point source by a sphere immersed in a potential flow is described in section III. The attractive feature of this technique is its simplicity. There are other advantages of using boundary element methods to solve this problem. These will become apparent in section III. In section IV boundary element solutions for two-dimensional models and comparisons with analytical models are presented. Calculations for a three-dimensional Silent Aircraft airframe are presented in section V. At high acoustic frequencies, boundary element methods become increasingly demanding (computationally). Thus boundary element calculations are restricted to low frequencies. These low frequency calculations provide a lower bound for the acoustic shielding estimates. A physically based model is used to extend the range of validity of the low-frequency solutions to higher frequencies and thus to estimate the reduction in OASPL. Accurate high-frequency solutions can be obtained by ray-acoustics methods, which is the subject of the on-going research work.

American Institute of Aeronautics and Astronautics

II.   Acoustic scattering

Consider a configuration in which fluid having a free-stream velocity of $\boldsymbol{u}_\infty$ flows past a fixed closed surface $\partial\Omega$. At low Mach numbers ($M^2 << 1$, where $M = |\bar{\boldsymbol{u}}|/c$ is the Mach number, $\bar{\boldsymbol{u}}$ is the local fluid velocity), the fluid-flow can be considered to be incompressible (see Batchelor,[7] pages 167–168). Also since variations in the speed of sound, c, depend on M^2, then correct to order M, c can be assumed to be a constant. Now if the fluid motion is assumed to be inviscid and irrotational, then the steady flow $\bar{\boldsymbol{u}}$ in the region Ω exterior to $\partial\Omega$ can be described by the Laplace equation

$$\nabla^2\bar{\phi} = 0 \tag{1}$$

with the requirement that the normal velocity on $\partial\Omega$ be zero. That is,

$$\boldsymbol{n}\cdot\nabla\bar{\phi} = 0 \text{ on } \partial\Omega \tag{2}$$

where $\boldsymbol{n}(\boldsymbol{x})$ is the unit inward normal at the point $\boldsymbol{x}$ on the surface $\partial\Omega$. Here $\bar{\phi}$ is the scalar velocity potential defined by $\bar{\boldsymbol{u}}(\boldsymbol{x}) = \nabla\bar{\phi}(\boldsymbol{x})$.

Equation (1) is the governing equation for the background (mean) flow. If this steady flow is disturbed by a small perturbation, the ensuing dynamics of the perturbed variables can be described by the continuity and momentum equations linearized about the equilibrium (mean/background) state given by the solution of Eq. (1). These linearized equations can then be manipulated such that for an acoustic source $S(\boldsymbol{x},t)$, the unsteady potential acoustic field can be represented by a single equation in terms of the perturbation acoustic potential ϕ. For a low Mach number mean flow, where terms of order M^2 are neglected, this equation is the convected wave equation (see Howe[8]):

$$\left(\frac{\partial}{\partial t} + \nabla\bar{\phi}\cdot\nabla\right)^2 \phi - c^2\nabla^2\phi = S(\boldsymbol{x},t). \tag{3}$$

For a rigid boundary, ϕ satisfies the boundary condition

$$\boldsymbol{n}\cdot\nabla\phi = 0 \text{ on } \partial\Omega. \tag{4}$$

Although in this analysis $\partial\Omega$ is assumed to be a rigid surface, it can be generalized easily for surfaces with arbitrary impedances. In the far field, ϕ satisfies the Sommerfeld radiation condition[9] that, in spherical coordinates (r,θ,ψ), can be written as

$$\lim_{r\to\infty}\left[r\left(\frac{\partial\phi}{\partial r} + \frac{1}{c}\frac{\partial\phi}{\partial t}\right)\right] = 0 \tag{5}$$

To illustrate the solution technique, consider the time-harmonic Green's function $\phi_g(\boldsymbol{x},t)$ that satisfies

$$\left(\frac{\partial}{\partial t} + \nabla\bar{\phi}\cdot\nabla\right)^2 \phi_g - c^2\nabla^2\phi_g = \delta(\boldsymbol{x}-\boldsymbol{x_o})\exp(-\mathrm{i}\omega t). \tag{6}$$

The space-time Green's function, g, can be obtained by the following inverse Fourier transform

$$g(\boldsymbol{x}-\boldsymbol{x_o},t-t_o) = \frac{1}{2\pi}\int_{-\infty}^{\infty}\phi_g(\boldsymbol{x}-\boldsymbol{x_o},t)\exp(\mathrm{i}\omega t_o)\mathrm{d}\omega. \tag{7}$$

The solution to Eq. (3) is then given by a convolution of the space-time Green's function with the source $S(\boldsymbol{x},t)$.

Using Taylor's transformations (see Taylor[5]):

$$\boldsymbol{X} = \boldsymbol{x}, \quad T = t + \bar{\phi}/c^2, \tag{8}$$

American Institute of Aeronautics and Astronautics

$\phi_g(\boldsymbol{x}, t) = \Phi(\boldsymbol{X}, T)$, and neglecting terms of order M^2, where $M = |\nabla\bar\phi|/c$ is the Mach number, Eq. (6) transforms into

$$\left(\frac{\partial^2}{\partial T^2} - c^2\nabla_X^2\right)\Phi = \delta(\boldsymbol{X} - \boldsymbol{X_o})\exp[i\omega\bar\phi(\boldsymbol{X})/c^2]\exp[-i\omega T]. \tag{9}$$

where $\nabla_X^2 = \partial^2/\partial X_i\partial X_i$. The boundary condition (4) transforms into

$$\boldsymbol{n}\cdot\left(\nabla_X\Phi + \frac{1}{c^2}\nabla\bar\phi\frac{\partial\Phi}{\partial T}\right) = 0 \text{ on } \partial\Omega. \tag{10}$$

Upon substituting Eq. (2), the transformed boundary condition reduces to

$$\boldsymbol{n}\cdot\nabla_X\Phi = 0 \text{ on } \partial\Omega. \tag{11}$$

Since the large time-asymptotic response is expected to be time-harmonic at the source frequency, the assumption $\Phi(\boldsymbol{X}, T) = \hat\Phi(\boldsymbol{X};\omega)\exp[-i\omega T]$ simplifies Eq. (9) into

$$\left(-\omega^2 - c^2\nabla_X^2\right)\hat\Phi = \delta(\boldsymbol{X} - \boldsymbol{X_o})\exp[i\omega\bar\phi(\boldsymbol{X})/c^2]. \tag{12}$$

The operator on the left-hand side is the familiar Helmholtz operator. Let the Green's function for the Helmholtz equation be given by

$$\left(-\omega^2 - c^2\nabla_X^2\right)\hat\Phi_h(\boldsymbol{X}|\boldsymbol{X_s}) = \delta(\boldsymbol{X} - \boldsymbol{X_s}), \tag{13}$$

with $\hat\Phi_h$ satisfying the boundary condition

$$\boldsymbol{n}\cdot\nabla_X\hat\Phi_h = 0 \text{ on } \partial\Omega. \tag{14}$$

Then the solution to Eq. (12) is given by

$$\hat\Phi(X;\omega) = \hat\Phi_h(\boldsymbol{X}|\boldsymbol{X_o})\exp[i\omega\bar\phi(\boldsymbol{X_o})/c^2]. \tag{15}$$

Transforming back to the original variables, the time-harmonic Green's function is given by

$$\phi_g(\boldsymbol{x}, t) = \hat\Phi_h(\boldsymbol{x}|\boldsymbol{x_o})\exp\{i\omega[\bar\phi(\boldsymbol{x_o}) - \bar\phi(\boldsymbol{x})]/c^2\}\exp(-i\omega t). \tag{16}$$

The acoustic pressure is related to the perturbation potential via the Bernoulli equation

$$p(\boldsymbol{x}, t) = -\bar\rho\left(\frac{\partial\phi}{\partial t} + \nabla\bar\phi\cdot\nabla\phi\right), \tag{17}$$

where $\bar\rho$ is the free-stream mean density.

With the acoustic potential given by Eq. (16), the acoustic pressure, correct to order M^2, can be written as

$$p(\boldsymbol{x}, t) = -\bar\rho\left(-i\omega\hat\Phi_h + \nabla\bar\phi\cdot\nabla\hat\Phi_h\right)\exp\{i\omega[\bar\phi(\boldsymbol{x_o}) - \bar\phi(\boldsymbol{x})]/c^2\}\exp(-i\omega t). \tag{18}$$

Note that $\hat\Phi_h$ is independent of the mean flow. Its effect on the acoustic pressure is displayed, explicitly, through terms involving $\bar\phi(\boldsymbol{x})$.

III. Boundary element formulation

The boundary element implementation for the acoustic scattering problem involves a two-step process. From Eq. (16) it can be seen that the magnitude of the complex acoustic potential is given by the solution of the Helmholtz equation and the phase is a function of the mean flow. Since $\hat\Phi_h$ is independent of the

mean flow, the acoustic potential and consequently the acoustic pressure field can be evaluated by solving, independently, the Helmholtz equation [(13) and (14)] and the Laplace equation [(1) and (2)]. Boundary element methods for solving these equations are readily available. Thus the effect of low-Mach number homentropic potential flows on acoustic scattering problems can be obtained by using existing boundary element software. Since acoustic and mean flow calculations become decoupled, a single acoustic boundary-element calculation can be used to investigate a variety of mean flows, such as, flows with different Mach numbers past airfoils at different angles of attack (if the source position remains fixed relative to the airfoil). Note that the mean-flow velocity potential need only be known at the source and observer positions. Hence, boundary element methods are well-suited for solving the Laplace equation because they allow for point-wise computation of the flow field. There are other advantages of using boundary element methods. Radiation boundary conditions are implicitly satisfied and only the external surfaces of enclosed bodies in the domain (not the entire domain) need to be discretized. For problems in which there are several source locations but few observer locations of interest, an adjoint formulation can be used. This has a big computational advantage because the sound-propagation problem from multiple sources can be solved by a single calculation. It can be shown easily that the adjoint equation can be obtained from the direct equation (6) by just reversing the direction of the mean flow. Hence the same procedure described above with $\bar{\phi}$ replaced with $-\bar{\phi}$ can be used to obtain the adjoint solution.
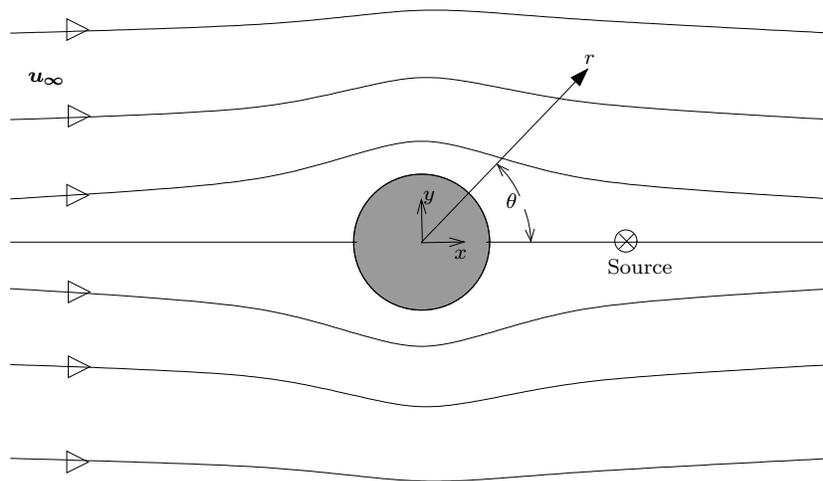
Figure 1. An axial plane of a sphere immersed in a stream with a uniform velocity at infinity. An acoustic monopole source is located on the x-axis

A.   Acoustic scattering from a point source by a sphere immersed in a potential flow

To illustrate the application of the boundary element method, we consider the example of the scattering of acoustic waves from a point source by a rigid sphere. Let the sphere of radius a be located at the origin and a point source be located on the x-axis at a distance r_s from the origin. The sphere is immersed in a flow with a uniform value of u_∞ in the $+x$ direction at infinity. Thus both the mean flow and acoustic fields are axisymmetric about the x-axis. These fields can be described adequately by a spherical polar coordinate system (r, θ, ψ), as shown in Fig. 1.

As seen from Eq. (18) the pressure field for this problem requires a solution of both Helmholtz and Laplace equations. The solution of Laplace equation for this problem is well known and is given by (for a

American Institute of Aeronautics and Astronautics
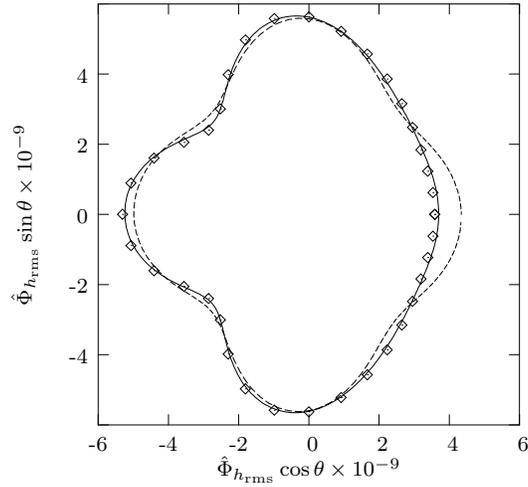
Figure 2. Directivity pattern for $\hat{\bar{\Phi}}_h$ ($ka = 2$, $kr_s = 4$, $kr = 200$. ———, 10 points per wavelength; $---$, 6 points per wavelength;$\diamondsuit$, analytical solution)

more general geometry, the solution could be obtained numerically by a boundary element method):

$$\bar{\phi}(r,\theta) = u_\infty \cos\theta \left(\frac{a^3}{2r^2} + r \right), \tag{19}$$
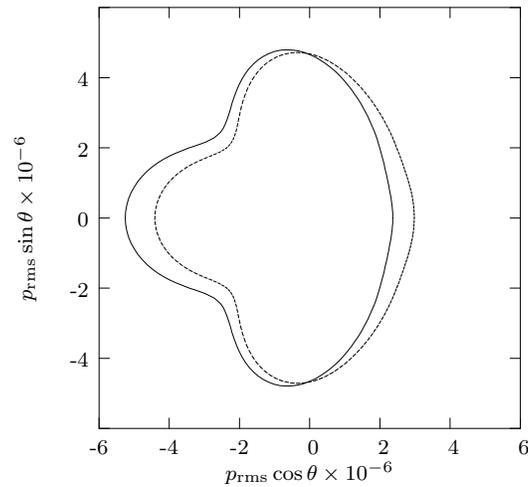
Figure 3. Sound directivity pattern in the axial plane of the sphere (———, $u_\infty = 0.2\,c$; $---$, $u_\infty = 0$)

The solution to Helmholtz equation $(\hat{\bar{\Phi}}_h)$ is obtained by using COMET/Acoustics.[10] The surface of the sphere is discretized by MSC/Patran.[11] Figure 2 compares the directivity pattern for $\hat{\bar{\Phi}}_h$ at a distance of $kr = 200$, where $k = \omega/c$ is the source wavenumber, for different mesh resolutions, with the analytical solution. It can be seen that about ten mesh points per acoustic wavelength are adequate to yield a converged solution (cf. Agarwal and Morris[12]). The parameters chosen for this calculation are $ka = 2$, $kr_s = 4$,

American Institute of Aeronautics and Astronautics

$u_\infty = 0.2\,c$.

Once $\bar{\phi}$ and $\hat{\Phi}_h$ are known the acoustic pressure field is obtained from Eq. (18). Figure 3 shows the sound directivity pattern in the axial plane at a distance of $k\,r = 200$. Also shown in the figure is the sound directivity pattern when the fluid is stationary. It can be seen the flow-field enhances the pressure field in upstream directions and reduces it in downstream directions. Taylor[5] showed that the mean flow introduces a single Doppler factor $(1 - M_\infty \cos\theta)$ in the far-field expression for pressure, which explains the observed directivity patterns. A slightly modified derivation is presented here for completeness. In the far field, Eq. (18) can be simplified by noting that correct to order $1/r$,

$$\bar{\phi} = u_\infty r \cos\theta, \text{ and} \tag{20}$$

$$\nabla^2 \hat{\Phi}_h = \frac{1}{r^2}\frac{\partial}{\partial r}\left(r^2 \frac{\partial \hat{\Phi}_h}{\partial r}\right) \tag{21}$$

Using (21), correct to order $1/r$, (13) can be written as

$$-\omega^2 \hat{\Phi}_h - c^2 \frac{1}{r^2}\frac{\mathrm{d}}{\mathrm{d}r}\left(r^2 \frac{\mathrm{d}\hat{\Phi}_h}{\mathrm{d}r}\right) = 0 \tag{22}$$

The outgoing wave solution to this equation is given by

$$\hat{\Phi}_h = \Lambda \frac{\exp[\mathrm{i}kr]}{r}, \tag{23}$$

where Λ is independent of r. Upon substituting Eqs. (20) and (23) in Eq. (18) and neglecting terms of order $1/r^2$ it can be shown that

$$|p(\boldsymbol{x}, t)| = \omega \bar{\rho} \hat{\Phi}_h (1 - M_\infty \cos\theta), \tag{24}$$

where M_∞ is the free-stream Mach number. Equation (24) gives the effect of a potential mean flow on the far-field acoustic pressure amplitude. Note that this simple expression of single Doppler factor in the far-field expression for pressure is applicable only for a monopole source. For realistic sources, the effect of the flow field on the sound directivity pattern would be more complex. The mean-flow convection effects for an arbitrary source distribution $\hat{S}(\boldsymbol{x})$ can be found by forming a convolution of the Green's function given by Eq. (16) with $\hat{S}(\boldsymbol{x})$. That is,

$$\begin{aligned}\phi(\boldsymbol{x}; \omega) &= \int \phi_g(\boldsymbol{x}|\boldsymbol{x_o}; \omega)\hat{S}(\boldsymbol{x_o})\mathrm{d}\boldsymbol{x_o} \\ &= \mathrm{e}^{-\mathrm{i}\omega\bar{\phi}(\boldsymbol{x})/c^2} \int \hat{\Phi}_h(\boldsymbol{x}|\boldsymbol{x_o}) \exp[\mathrm{i}\omega\bar{\phi}(\boldsymbol{x_o})/c^2]\hat{S}(\boldsymbol{x_o})\mathrm{d}\boldsymbol{x_o}.\end{aligned} \tag{25}$$

Defining a modified source distribution $\hat{S}'(\boldsymbol{x}) = \hat{S}(\boldsymbol{x})\exp[\mathrm{i}\omega\bar{\phi}(\boldsymbol{x})/c^2]$, Eq. (25) can be written as

$$\phi(\boldsymbol{x}; \omega) = \mathrm{e}^{-\mathrm{i}\omega\bar{\phi}(\boldsymbol{x})/c^2}\left[\int \hat{\Phi}_h(\boldsymbol{x}|\boldsymbol{x_o})\hat{S}'(\boldsymbol{x_o})\mathrm{d}\boldsymbol{x_o}\right]. \tag{26}$$

The term in the parenthesis is the solution of the Helmholtz equation for the modified source distribution $\hat{S}'(\boldsymbol{x})$, which can be obtained by the boundary element software. Finally, the pressure field is obtained by the application of Bernoulli's equation (18).

IV. Two-dimensional models

We expect that for an acoustic source placed above the wing, there would be a significant reduction of noise in the shadow region underneath the wing. In order to understand the effect of various parameters

American Institute of Aeronautics and Astronautics
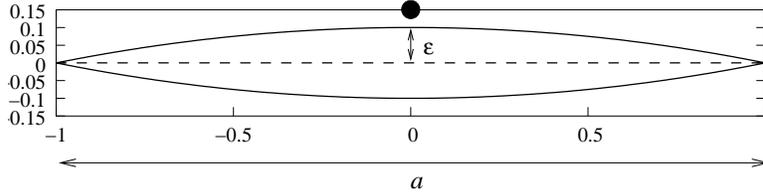
Figure 4. Schematic for the set-up for acoustic scattering from a point source by flat plate ($-- --$) and a biconvex ellipse (——)

such as wing thickness, edge curvatures, source location and frequency, we have analyzed two sets of two-dimensional wing models. One consisting of a flat plate and a biconvex ellipse with sharp edges, as shown in Fig. 4, and the other consisting of an ellipse and a Zhukovsky airfoil, shown in Fig. 5. These models have a chord length of $a = 2$ m. The ellipses have a maximum thickness of $\epsilon = 0.05\,a$. The radius of curvature of the edge of the ellipse in Fig. 5, $\rho = \epsilon^2$, is chosen so as to match that of the leading edge of the airfoil. A time-harmonic point acoustic source is placed at $(0, 1.5\epsilon)$. The source frequency is chosen such that the Helmholtz number, $ka = 50$, where k is the wavenumber of the source. This Helmholtz number corresponds to the fundamental frequency of the fan of the Silent Aircraft engine, which is the lowest tonal frequency of interest. Since we expect more shielding at higher frequencies (as explained below), the present analysis provides a lower bound on the shielding estimates.
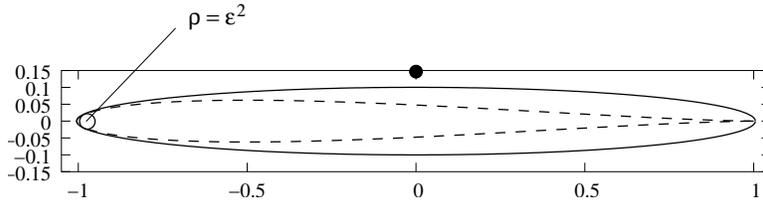
Figure 5. Schematic for the set-up for acoustic scattering from a point source by Zhukovsky airfoil ($-- --$) and an ellipse (——)

The two-dimensional acoustic shielding problem is solved by a boundary-element solver.[12] Since the wave equation is separable in elliptical coordinates, an analytical solution can be obtained for the ellipse and the flat-plate, which is a zero-thickness ellipse. The analytical solution is given in Appendix A. It is consistent with the boundary-element solution. Figure 6 shows the sound directivity pattern for the flat-plate and biconvex-ellipse. Also shown is the directivity pattern for the incident field from the source. It can be seen that there is a reduction of noise by about 13 dB noise reduction underneath the wing compared with the incident field. The directivity pattern has some interesting features. There are wiggles (lobes) in the shadow region underneath the wing, which are almost identical for the flat-plate and the biconvex-ellipse. There are dips in the directivity pattern above, for the flat plate. The dips are due to the interference between the direct and reflected waves between the source and the observer. This can be seen easily by placing an image source below the flat plate that is of the same strength and is equidistant from the plate. The image source accounts for the reflected waves from the upper surface of the wing. The sound field obtained by adding the contribution from the source and image, shown in Fig. 7, has dips in the directivity pattern at the same location as that given by the boundary-element solution. The dips disappear for the biconvex-ellipse case because in that case the source is closer to the surface, hence the source and image pair being closer compared to a wavelength, behave nearly as a single source. The wiggles underneath are due to the interference from the diffracted field from the two edges. The high value for the Helmholtz number ($ka = 50$) indicates that

American Institute of Aeronautics and Astronautics
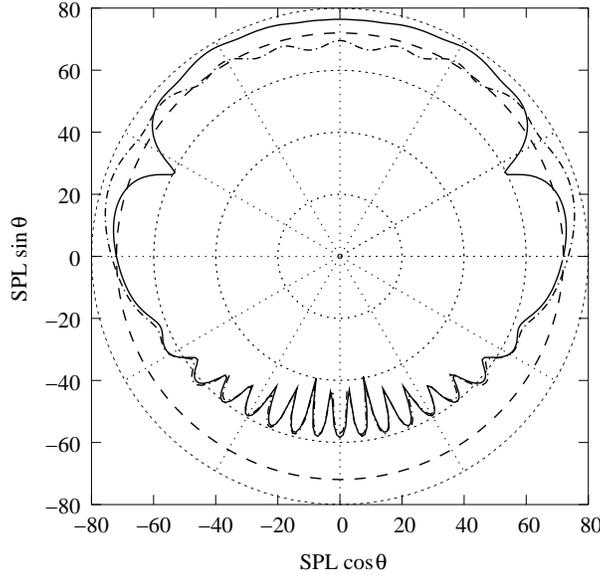
Figure 6. Sound directivity pattern from the flat plate (——), biconvex cylinder ($-\cdot-\cdot-\cdot$), and the incident field ($------$)

the acoustic wavelength is small compared with the chord-length. Therefore, for the length scales associated with this problem, the frequency is high and hence ray-theory results are applicable. The two-dimensional diffracted field from the edge of a wedge with exterior angle β is given by (see Appendix B and Fig. 14)

$$\hat{p}_{2D} = \frac{\hat{S}}{k}\frac{\pi}{\beta}\frac{\mathrm{i}}{\sqrt{rr_s}}\mathrm{e}^{\mathrm{i}k(r+r_s)}D_\nu(\phi,\phi_s) \qquad (27)$$

where (r,ϕ) and (r_s,ϕ_s) are the locations of the observer and source, respectively, in polar coordinates with the origin at the edge, $\hat{S}$ is the source strength and $D_\nu(\phi,\phi_s)$ is the directivity function defined in Eq. (40). The total diffracted field in the shadow region, given by adding the contributions from the two edges, is shown in Fig. 7. The interference pattern from the diffracted field matches the directivity pattern underneath the plate obtained from the boundary element solutions. Note that the only difference in the expression for the diffracted field between the flat-plate and the biconvex ellipse is the external wedge angle β. For the flat plate, $\beta = 2\pi$, which is nearly the same for the biconvex ellipse. This explains why the diffracted field for the two cases is similar. It can be seen from Eq. (27) that the diffracted pressure field in the shadow region is inversely proportions to frequency. Thus, if the frequency is doubled, SPL reduces approximately by 6 dB. Note that doubling the frequency would double the number of lobed patterns, but, averaged over a wavelength, the SPL would reduce by 6 dB. In three-dimensions, the diffracted pressure field is inversely proportional to square root of frequency [see Eq. (39)]. Thus doubling the frequency would reduce the SPL by approximately 3 dB.

Figure 8 shows the sound directivity pattern for the ellipse and the Zhukovsky airfoil. The directivity pattern looks similar to the flat-plate and biconvex-ellipse case, even though the Zhukovsky airfoil has a rounded leading-edge and the ellipse has rounded leading and trailing edges. This indicates that the sharp-edge diffraction mechanism is applicable also to the rounded-edged models. This is because the radius of curvature, ρ, is small compared with the wavelength ($k\rho = 0.25$). However, as the frequency of the source increases, $k\rho$ would become larger and the diffraction mechanism would change from a sharp-edge to a creeping-ray mechanism. The pressure field due to sharp-edge diffraction falls linearly with increasing

American Institute of Aeronautics and Astronautics
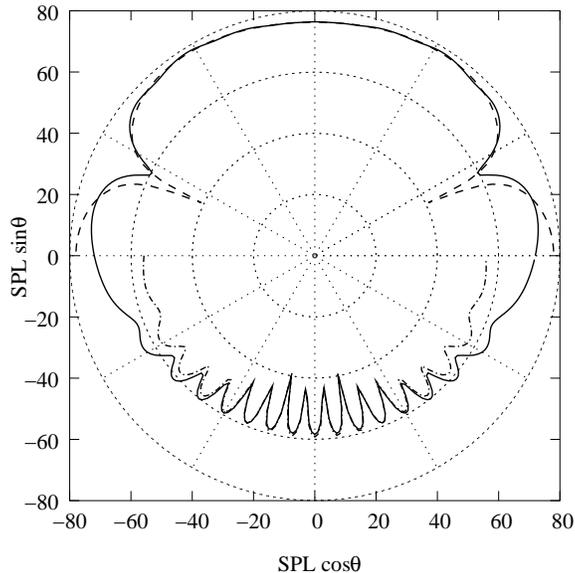
Figure 7. Comparison between the interference pattern obtained from the image-source model (− − −−) and the diffraction field in the shadow zone (− · − · −·) with the boundary-element solution (——)

frequency, whereas it decays exponentially for a creeping wave. Thus for rounded edges with non-negligible $k\rho$, a significantly higher reduction of sound in the shadow region can be expected. This is the subject of ongoing research work in which high frequency acoustic scattering is being calculated by ray tracing techniques.

In order to determine the effect of source location on the amount of shielding in the shadow region, it is appropriate to solve the adjoint problem. Fig. 9 shows the adjoint sound field above the Zhukovsky airfoil for three source locations in the far field. In polar coordinates, the sources are located at $kr = 500$ and $\theta = -90\,\mathrm{deg}$, $-60\,\mathrm{deg}$ and $-120\,\mathrm{deg}$. Because of the reciprocity between the adjoint and direct fields, the adjoint sound field at an observer location above the airfoil from a source in the far field is the same as the direct sound field from the source located above the airfoil and the observer in the far-field. That is $p(\boldsymbol{x}|\boldsymbol{x_s}) = p_a(\boldsymbol{x_s}|\boldsymbol{x})$, where p and p_a are the direct and adjoint fields, respectively, $\boldsymbol{x} \equiv (r, \theta)$ is the observer location and $\boldsymbol{x_s}$ is the source location. Fig. 9 also shows the adjoint incident field from the farfield source located at $\theta = -90\,\mathrm{deg}$. In general, the amount of shielding is a function of the relative locations of source and observers with respect to the edge. It can be seen that unless the source is located very close to the edges, significant amount of shielding is obtained in all directions. This can be explained based on the edge-diffraction theory. If there is no direct line of sight between the source and observer then the observer is in the shadow region and it receives a weak diffracted field from the edges.

V. Acoustic shielding by a Silent Aircraft

Acoustic shielding effects are estimated by means of a monochromatic point acoustic source placed above the airframe of Silent Aircraft Experimental (SAX03). Figure 10 shows the orthographic projections of the SAX03 airframe. The source is located at $(2/3a, 0.05a, 0)$, where a is the center-body chord length.

Figure 11 shows the far-field sound directivity patterns in the $x - y$ plane at three spanwise locations: $z = 0$, $z = b/2$, and $z = b$, where b is the wingspan. Also shown is the incident field from the source on the plane $z = 0$. The source frequency corresponds to a Helmholtz number, $ka = 50$. This frequency

American Institute of Aeronautics and Astronautics
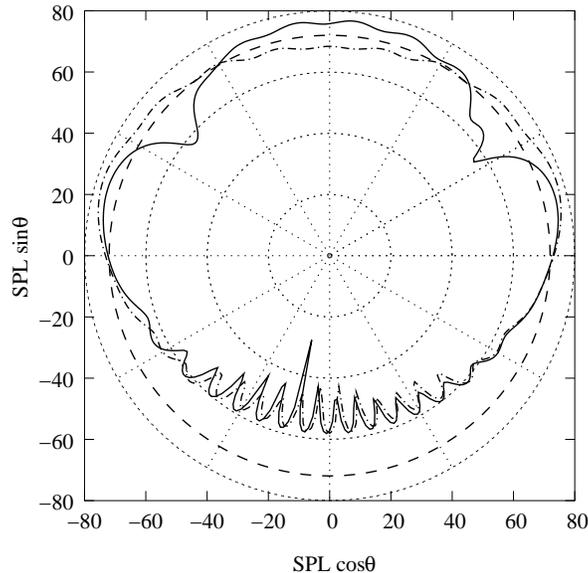
Figure 8. Sound directivity pattern from an ellipse ($- \cdot - \cdot -\cdot$) and a Zhukovsky airfoil (——)

corresponds to the fundamental frequency of the fan.[14] It can be seen that a reduction of at least 5 dB is obtained in the shadow region underneath the aircraft. In dimensional terms, the frequency of the source for this calculation is approximately 50 Hz. The human ear is fairly insensitive at such low frequencies. At higher frequencies, where are ears are more sensitive, we expect a greater amount of noise reduction due to shielding as explained in the preceding section. After finding the pressure field in the shadow region at 50 Hz, we have made use of the inverse square-root dependence of pressure on frequency to extend the solution to higher frequencies. Averaged over a wavelength this procedure is expected to yield a reasonable approximation. The average acoustic intensities in the various frequency bands can be added after applying the A-weighting filter function, which provides a reasonable representation of how the human ear perceives loudness, to get the OASPL in dBA. Fig. 12 shows the relative effects of shielding for the OASPL in dBA for forward propagating fan noise at various angles. It can be seen that there is at least an 18 dB reduction of sound due to shielding. Thus the airframe provides a significant amount of shielding for the overall perceived noise levels.

VI.   Conclusions

Acoustic shielding of low-frequency engine noise by the Silent Aircraft airframe has been investigated by solving an external acoustic scattering problem. By means of Taylor's transformation, the governing equations for sound propagation through homentropic potential flows at low Mach numbers can be transformed into an ordinary wave equation. For external acoustic scattering problems from time harmonic sources, Taylor's transformation decouples the mean flow and acoustic field calculations. The acoustic potential field can then be obtained by solving, independently, the Helmholtz and Laplace equations. This technique is amenable to solving both direct and adjoint sound propagation problems. Boundary element methods offer a simple and efficient way of solving these equations at low frequencies. Analysis of simple two-dimensional models has shown that there are two important length scales in the scattering problem: the chord length and the radius of curvature of the edges. For the engine frequencies in the audible range, even the lowest frequency corresponds to an acoustic wavelength that is much smaller than the chord length. This means

American Institute of Aeronautics and Astronautics
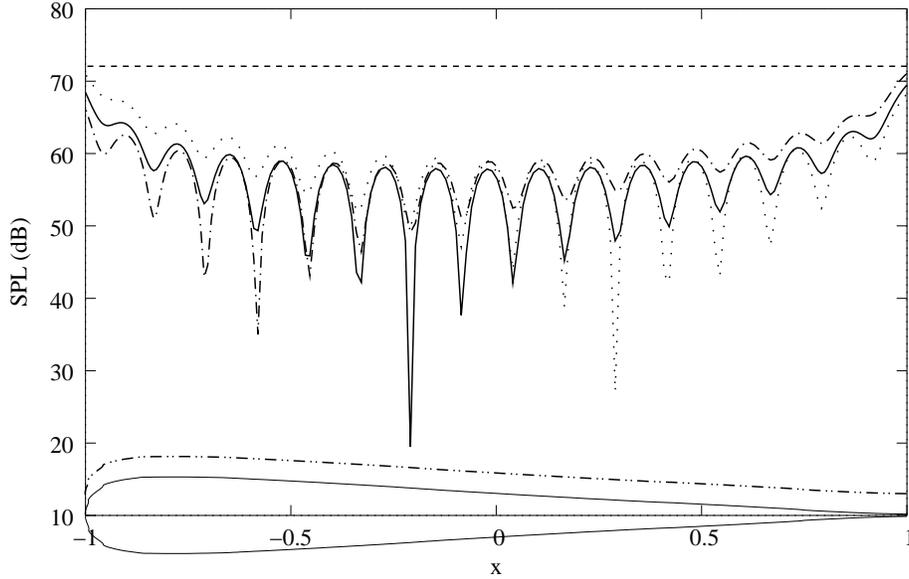
Figure 9. SPLs for the adjoint acoustic field at a location $(-\cdot\cdot-\cdot\cdot-)$ **above the Zhukovsky airfoil for three far-field source locations:** ———, $\theta = -90\,\deg$; $-\cdot-\cdot-\cdot$, $\theta = -60\,\deg$; $\cdots\cdots$, $\theta = -120\,\deg$; $-\,-\,-\,-$, **Incident field**

that models based on ray theory can be used to to get better physical insight into the boundary element solutions. It has been observed that if the radius of curvature of an edge is small compared to an acoustic wavelength, the edge behaves as a sharp edge. If there is no direct line of sight between a source above the wing and an observer underneath, then the observer is in a shadow region where there is a significant amount of noise reduction. The sound pressure field in the shadow region is inversely proportional to frequency for two-dimensional problems and to square root of frequency for three-dimensional problems. Therefore, acoustic shielding becomes more effective at higher frequencies. Low-frequency calculations of acoustic shielding from a monopole source, pulsating at the fundamental fan frequency, placed above a Silent Aircraft airframe show a significant amount of shielding (at least 5dB) throughout the shadow region. The present analysis provides a framework for predicting noise from realistic sources. Boundary element methods become increasingly demanding of computational resources at high frequencies. To complement the boundary element method at high frequencies, a solution procedure based on ray acoustics is being developed.

Appendix

A.   Acoustic scattering from an ellipse

The time-harmonic Green's function satisfies the Helmholtz equation

$$(\nabla_X{}^2 + k^2)G(\boldsymbol{r}|\boldsymbol{r_o};\omega) = -4\pi\delta(\boldsymbol{r} - \boldsymbol{r_o}) \tag{28}$$

Consider an elliptic coordinate system (see Fig. 13) defined by

$$
\begin{aligned}
x &= a/2\cosh\mu\cos\nu \\
y &= a/2\sinh\mu\sin\nu
\end{aligned}
\tag{29}
$$

The incident field from the point source can be expanded in terms of a series in elliptical coordinates (see

American Institute of Aeronautics and Astronautics
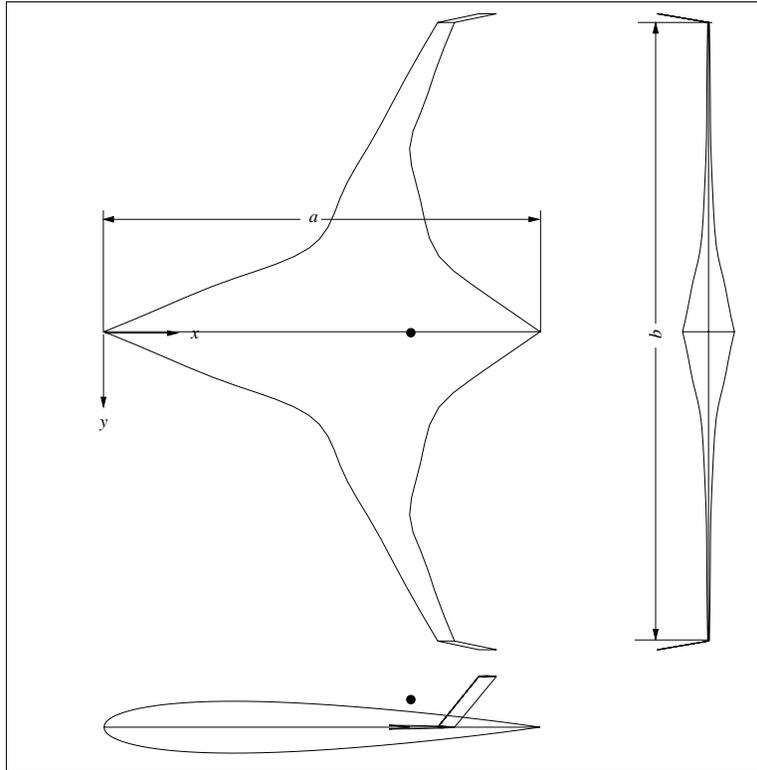
Figure 10. Orthographic projections of the Silent Aircraft airframe SAX03 (from Diedrich[13])

page 1421, Morse and Feshback[15])

$$
\begin{aligned}
G^I(\boldsymbol{r}|\boldsymbol{r_o};\omega) \;=\;& \mathrm{i}\pi \mathrm{H}_0^{(1)}(kR) \\[2mm]
\;=\;& 4\pi\mathrm{i}\left\{\sum_{m=0}^{\infty}\left[\frac{Se_m(h,\cos\nu_o)}{M_m^e(h)}\right]Se_m(h,\cos\nu)\right. \\[2mm]
& \qquad\left\{\begin{array}{l} Je_m(h,\cosh\mu_o)He_m(h,\cosh\mu);\ \ \mu>\mu_o \\ Je_m(h,\cosh\mu)He_m(h,\cosh\mu_o);\ \ \mu_o>\mu \end{array}\right. \\[2mm]
& +\sum_{m=1}^{\infty}\left[\frac{So_m(h,\cos\nu_o)}{M_m^o(h)}\right]So_m(h,\cos\nu) \\[2mm]
& \qquad\left.\left\{\begin{array}{l} Jo_m(h,\cosh\mu_o)Ho_m(h,\cosh\mu);\ \ \mu>\mu_o \\ Jo_m(h,\cosh\mu)Ho_m(h,\cosh\mu_o);\ \ \mu_o>\mu \end{array}\right.\right\},
\end{aligned}
$$

$$(30)$$

where

$$
\begin{aligned}
He_m &= Je_m + \mathrm{i}Ne_m \\
Ho_m &= Jo_m + \mathrm{i}No_m
\end{aligned}
$$

$$(31)$$

are solutions corresponding to outgoing waves, Se_m, So_m are even and odd Mathieu functions, respectively, of order m; $M_m^e(h)$, $M_m^o(h)$ are the normalization constants for these functions; Je_m, Jo_m are the even and

American Institute of Aeronautics and Astronautics
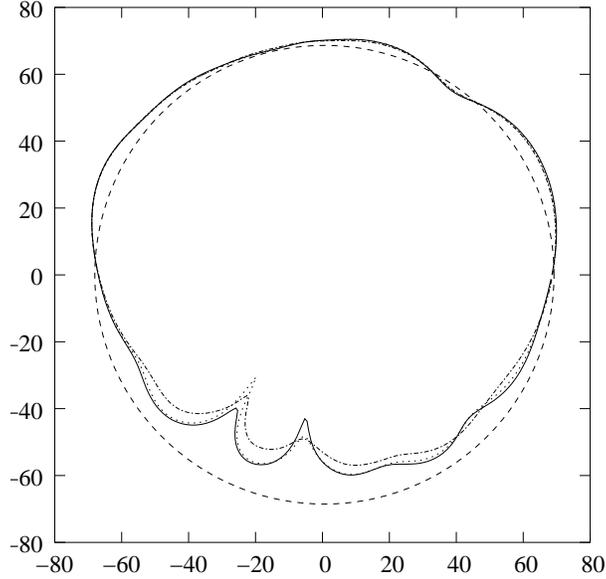
Figure 11. Sound directivity pattern in the far field ($kr = 500$) for SAX03. $----$, incident field; ———, $z = 0$; $\cdots\cdots$, $z = b/2$; $-\cdot-\cdot-\cdot$, $z = b$

odd radial Mathieu functions of the first kind; and Ne_m, No_m are the even and odd radial Mathieu functions of the second kind.

The scattered field can be represented as

$$G^S(\mu, \nu | \mu_o, \nu_o) = \sum_{m=0}^{\infty} A_m^e(\mu_o, \nu_o) Se_m(h, \cos \nu) He_m(h, \cosh \mu) + \sum_{m=1}^{\infty} A_m^o(\mu_o, \nu_o) So_m(h, \cosh \nu) Ho_m(h, \cosh \mu)$$

(32)

$$\frac{\partial G^S}{\partial \mu}(\mu = 0) = \sum_{m=0}^{\infty} A_m^e Se_m(h, \cos \nu) Je_m(h, 1) + \sum_{m=1}^{\infty} A_m^o So_m(h, \cos \nu) Ho_m'(h, 1)$$

(33)

From Eq. (30),

$$\frac{\partial G^I}{\partial \mu}(\mu = 0) = 4\pi i \sum_{m=1}^{\infty} \left[\frac{So_m(h, \cos \nu_o)}{M_m^o(h)} \right] So_m(h, \cos \nu) Jo_m'(h, 1) Ho_m(h, \cosh \mu_o)$$

(34)

Since the normal velocity on the plate must be zero

$$\frac{\partial G^S}{\partial \mu}(\mu = 0) = -\frac{\partial G^I}{\partial \mu}(\mu = 0)$$

(35)

This gives

$$
\begin{aligned}
A_m^e &= 0 \\
A_m^o &= -4\pi i \left[\frac{So_m(h, \cos \nu_o)}{M_m^o(h)} \right] \frac{Jo_m'(h, 1)}{Ho_m'(h, 1)} Ho_m(h, \cosh \mu_o)
\end{aligned}
$$

(36)

Hence

$$G^S = -4\pi i \frac{Jo_m'(h, 1)}{Ho_m'(h, 1)} \left[\frac{So_m(h, \cos \nu_o)}{M_m^o(h)} \right] So_m(h, \cos \nu) Ho_m(h, \cosh \mu_o) Ho_m(h, \cosh \mu)$$

(37)

American Institute of Aeronautics and Astronautics
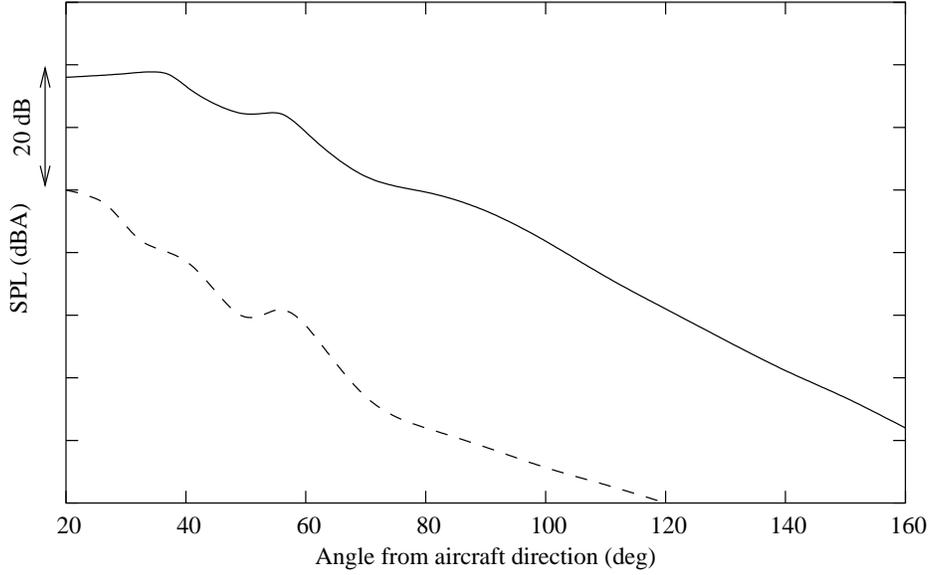
Figure 12. Effect of shielding on forward-propagating fan noise at various observer angles in the farfield. ——, fan noise without shielding; − − −−, fan noise with shielding.

Finally

$$G(\boldsymbol{r}|\boldsymbol{r_o};\omega) = G^I + G^S \tag{38}$$

B. Diffracted field from a two-dimensional edge

Consider a rigid wedge with a sharp edge. The edge of the wedge coincides with the z-axis. Let the observer location in a cylindrical coordinate system be given by (r,ϕ,z), where the polar angle $\phi = 0$ corresponds to one of the faces of the wedge and $\phi = \beta$ corresponds to the other face, as shown in Fig. 14. A time-harmonic monopole source of amplitude $\hat{S}$ and wavenumber k is located at (r_s,ϕ_s,z_s). The expression for the diffracted field by the edge of the wedge in a three-dimensional space is given by (see Pierce,[9] page 491)

$$\hat{p}_{3D} = \frac{\hat{S}}{2\beta}\left(\frac{2\pi}{kLrr_s}\right)^{1/2} e^{i(kL\pi/4)} D_\nu(\phi,\phi_s) \tag{39}$$

where

$$D_\nu(\phi,\phi_s) = \frac{\sin\nu\pi}{\cos\nu\pi - \cos\nu(\phi+\phi_s)} + \frac{\sin\nu\pi}{\cos\nu\pi - \cos\nu(\phi-\phi_s)}, \tag{40}$$

$L = \left[(r+r_s)^2 + (z-z_s)^2\right]^{1/2}$ is the shortest path around the edge from the source to the observer, and $\nu = \pi/\beta$ is the wedge index.

The corresponding diffracted field in two-dimensions can be obtained by replacing the point source by a line source of strength $\hat{S}$ per unit length. Then the two-dimensional diffracted field is given by

$$\hat{p}_{2D} = \int_{-\infty}^{\infty} \hat{p}_{3D}\mathrm{d}z_s \tag{41}$$

Without loss of generality z is chosen to be zero. This integrand has an exponential term with an imaginary argument. This can be integrated by the Method of Stationary Phase for large kL (or large kr). After

American Institute of Aeronautics and Astronautics
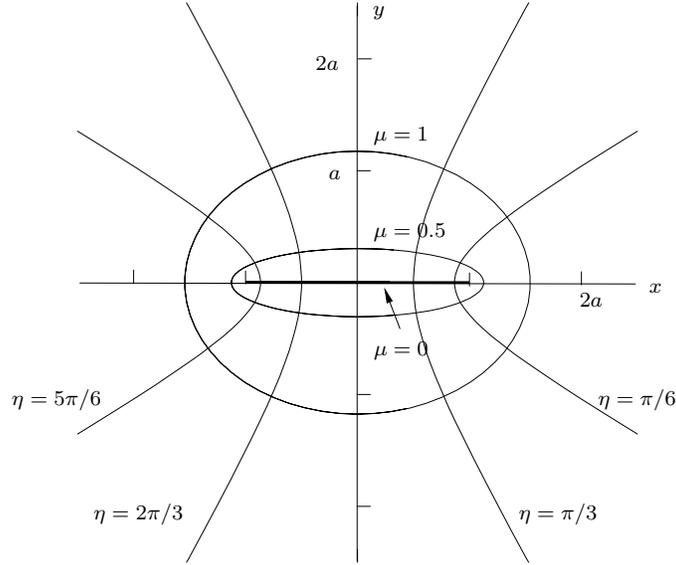
Figure 13. Elliptic coordinates used to evaluate the scattered field from a flat-plate ($\mu = 0$) and an ellipse

the application of the Method of Stationary Phase, the expression for the two-dimensional diffracted field is given by

$$\hat{p}_{2D} = \frac{\hat{S}}{k}\frac{\pi}{\beta}\frac{\mathrm{i}}{\sqrt{rr_s}}\mathrm{e}^{\mathrm{i}k(r+r_s)}D_\nu(\phi, \phi_s) \tag{42}$$

Acknowledgments

References

[1] Jeffery, R. W. and Holbeche, T. A., "Experimental studies of noise-shielding effects for a delta-winged aircraft," *AIAA Paper 75-513*, 1975.

[2] Clark, L. R. and Gerhold, C. H., "Inlet noise reduction by shielding for the blended-wing-body airplane," AIAA 99-1937, 1999.

[3] Gerhold, C. H., Clark, L. R., Dunn, M. H., and Tweed, J., "Investigation of Acoustical Shielding by a Wedge-Shaped Airframe," AIAA 2004-2866, 2004.

[4] Ricouard, J., Davy, R., Loheac, P., Moore, A., and Piccin, O., "ROSAS Wind Tunnel Test Campaign Dedicated to Unconventional Aircraft Concepts Study," AIAA 2004-2867, 2004.

[5] Taylor, K., "A Transformation of the Acoustic Equation with Implications for Wind-Tunnel and Low-Speed Flight Tests," *Proceedings of the Royal Society of London. Series A, Mathematical and Physical Sciences*, Vol. 363, No. 1713, 1978, pp. 271–281.

[6] Astley, R. J. and Bain, J. G., "A three-dimensional boundary element scheme for acoustic radiation in low Mach number flows," *Journal of Sound and Vibration*, Vol. 109, No. 3, 1986, pp. 445–465.

[7] Batchelor, G. K., *An Introduction to Fluid Dynamics*, Cambridge University Press, 1967.

[8] Howe, M. S., "The generation of sound by aerodynamic sources in an inhomogeneous steady flow," *Journal of Fluid Mechanics*, Vol. 67, 1975, pp. 597–610.

American Institute of Aeronautics and Astronautics
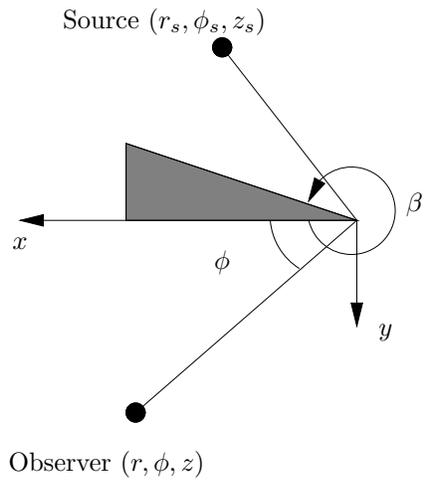
Figure 14. Parameters for diffraction from a sharp edge

[9]Pierce, A. D., *Acoustics, An Introduction to Its Physical Principles and Applications*, American Institute of Physics, 1994.

[10]COMET/Acoustics, *User's Manual*, Collins & Aikman, 2003.

[11]MSC/Patran, *User's Manual*, The MacNeaSchwendler Corporation, 2003.

[12]A. Agarwal and P. J. Morris, "Broadband noise from the unsteady flow in a slat cove," AIAA 2004-0854, 2004.

[13]Diedrich, A., *The Multidisciplinary Design and Optimization of an Unconventional, Extremely Quiet Transport Aircraft*, Master's thesis, Department of Aeronautics and Astronautics, MIT, Cambridge, MA, 2005.

[14]Hall, C. A. and Crichton, D., "Engine And Installation Configurations For A Silent Aircraft," ISABE 2005-1164, 2005.

[15]P. M. Morse and H. Feshbach, *Methods of Theoretical physics*, Vol. 2, McGraw Hill, 1953.